

A wind-tunnel study on exhaust gas dispersion from road vehicles—Part I: Velocity and concentration fields behind single vehicles

Isao Kanda^{a,*}, Kiyoshi Uehara^a, Yukio Yamao^a,
Yasuo Yoshikawa^{b,1}, Tazuko Morikawa^b

^a*National Institute for Environmental Studies, 16-2 Onogawa, Tsukuba, 305-8506, Japan*

^b*Petroleum Energy Center, 4-3-9 Toranomon, Minato-ku, Tokyo, 105-0001, Japan*

Received 1 December 2004; received in revised form 11 October 2005; accepted 6 December 2005

Available online 19 January 2006

Abstract

By a reduced-scale model in a wind tunnel, we investigate the dispersion behavior of exhaust gas from automobiles. Two types of vehicles are considered, a passenger car and a small-size truck. Tracer gas experiments show that the exhaust gas dispersion is enhanced significantly by the vehicle wake compared to the case when the vehicle body is absent. The passenger car and the truck promote dispersion in the horizontal and the vertical direction, respectively. The wake field is analyzed by particle image velocimetry (PIV), and the distribution of the mean and the fluctuation fields is found to conform to the concentration field of the exhaust gas. The buoyancy of the exhaust gas has minor effect except on the vertical spread behind the truck whose wake flow amplifies the vertical displacement generated near the pipe exit.

© 2005 Elsevier Ltd. All rights reserved.

Keywords: Air pollution; Traffic emissions; Wind tunnel; Particle image velocimetry; Exhaust buoyancy

1. Introduction

Automobile emission is a major source of air pollution in urban areas. In order to secure clean air, significant efforts have been made in improving fuel and engine technology, city

*Corresponding author. Tel.: +81 29 850 2765; fax: +81 29 850 2580.

E-mail address: kanda.isao@nies.go.jp (I. Kanda).

¹Nissan Research Center, 1 Natsushima-cho, Yokosuka, 237-8523 Japan.

planning, predictive models, and on-site monitoring. In this paper, we are concerned with predictive models, which despite many years of development, have not attained satisfactory reliability [1].

One of the sources of the prediction errors is the difficulty in representing the turbulence generated by the moving traffic. Previous models adopt widely varied approaches to incorporate the effect of traffic-produced turbulence on the pollutant dispersion. For example, an operational model CALINE4 [2] defines a *mixing zone* above the road, wherein the pollutant is emitted uniformly on the ground and dispersed by a uniform traffic-produced mechanical and thermal turbulence; another operational model, OMG volume-source model [3], assumes a finite volume above and separated from the road, which consists of a uniform distribution of point sources; a street-canyon model OSPM [4] relates the drag on vehicles to the production of turbulence kinetic energy; a CFD model by Yoshikawa and Kunimi [5] specifies enhanced eddy diffusivity in the vicinity of the road.

The variety of the modeling schemes stems from the paucity of knowledge about the effect of moving traffic on pollutant diffusion. Real-scale measurement, although desirable, is difficult because the effect of traffic movement and that of the ambient wind, which is seldom zero, are hard to separate. Numerical simulation has not reached the level to compute both the flow around a queue of moving vehicles and the diffusion of exhaust gas emitted from relatively narrow pipes, although exploratory works are emerging [6].

Wind-tunnel experiments, however, have offered valuable information. For the wake field behind a vehicle, there are numerous work at various scales including the real scale (e.g. [7,8]), but work on dispersion behavior is relatively rare. Eskridge and Rao [9] measured the concentration field of a tracer gas in the far wake (30–60 car-heights behind) of a model passenger car, and determined the optimal turbulence length scales for a predictive model ROADWAY. Clifford et al. [10] simulated a traffic congestion by three model passenger cars separated by half the car length. Because their primary concern was the air quality inside the vehicle, they measured the concentration distribution on the car surface including air inlet position. Their results suggested that the exhaust gas is dispersed significantly by the car immediately behind. Khare et al. [11] and Ahmad et al. [12] simulated traffic-produced turbulence by a ‘model vehicle movement system’ consisting of moving belts carrying model vehicles. The system was placed in various types of simulated atmospheric boundary layers, and the effect of the traffic condition and the wind direction on the vertical spread of the exhaust gas was examined.

In this paper, we present a wind-tunnel study of exhaust gas dispersion with an emphasis on the relationship between the velocity and the concentration fields. The velocity fields revealed by particle image velocimetry (PIV) enable us to explain the concentration fields in the relatively close vicinity of the vehicle. A novel feature of our experiments is the buoyancy of the exhaust gas, simulated by proper dynamical matching. For simplicity, we assume no ambient wind and no heat flux from vehicle engines, although they are both expected to have significant effects on the diffusion behavior. This paper focuses on single-vehicle configurations while our companion paper [13] deals with multi-vehicle configurations and discusses the traffic-produced turbulence.

2. Experimental method

We model a traffic condition typical of the Tokyo metropolitan area. A 12-h traffic survey was conducted on a weekday around Kamiyama intersection (Setagaya, Tokyo)

where the national highway 246 and the ring road No.7 crosses. For five drivers on a sedan-type passenger car, various driving parameters including speed, acceleration and inter-vehicle distance were monitored by on-vehicle instruments. The traffic consisted primarily of sedan-type passenger cars (P) and small-size trucks (T). Hence, these two types are tested in the wind-tunnel experiments. Fig. 1 shows the temporal frequency of the vehicle speed along the four routes branching from the intersection. On average, the frequency in the range between 10 and 40 km h⁻¹ was approximately uniform. For experimental convenience, an intermediate speed 20 km h⁻¹ (5.56 m s⁻¹) is selected. For simplicity, we consider a single lane, constant speed, no ambient wind and no heat flux from engines although interference between adjacent lanes, acceleration/deceleration, lateral wind, and natural convection due to engine heat are significant factors for exhaust gas diffusion.

Instead of vehicles moving into a still ambient, we study an equivalent situation with an approximately laminar wind blowing against stationary vehicles. Since we are concerned with steady state, the laws of dynamics are the same when viewed from the road-fixed frame and when viewed from the vehicle-fixed frame, which corresponds to our experiments. The experiments are conducted in the Atmospheric Diffusion Wind Tunnel at National Institute for Environmental Studies, Japan [14]. The test section is 2.6 m wide, 2.2 m high and 24 m long, and the measurements are done around the mid-length. The

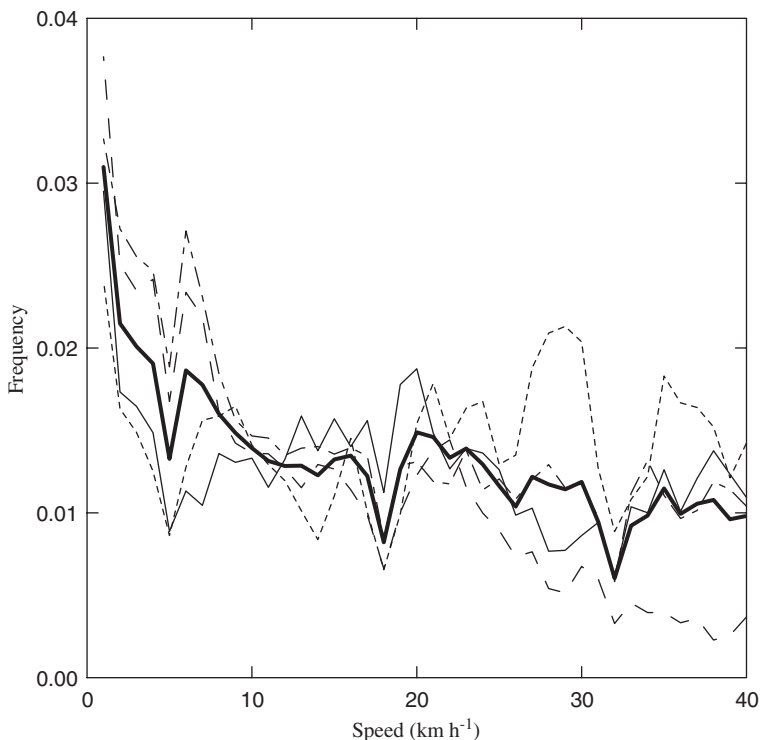


Fig. 1. Temporal frequency of the vehicle speed along the four routes branching from Kamiyuma intersection. The thin lines represent the data on individual routes, and the thick line the average. All the data are averages for five different drivers.

turbulence intensity at the center of the test section when the experimental setup is installed (see Fig. 3) is 2–3%.

The model size is $\frac{1}{20}$ of the real scale (Fig. 2). The exhaust pipes are installed at about the same positions as on the real vehicles. If the Reynolds number is to be matched for dynamical similarity, the wind speed U has to be 111 m s^{-1} , which is beyond the capacity of the wind tunnel and is also inconvenient for necessary measurements. Instead, we seek a critical value of U beyond which the velocity field around the vehicles remains similar.

In order to simulate the buoyancy of the hot exhaust gas, we use a mixture of ethane (C_2H_6), helium (He) and nitrogen (N_2), where ethane is the tracer gas whose concentration behind the vehicles is measured by a flame ionization detector (FID), helium controls the buoyancy, and nitrogen dilutes the gas so that the ethane concentration is within the dynamic range of FID. The buoyancy, or the ratio of helium, of the exhaust gas is determined by matching the Froude number Fr defined by

$$Fr = \sqrt{\frac{\rho_a U^2}{(\rho_a - \rho_e)gD}}, \quad (1)$$

where ρ_a is the density of the ambient air, ρ_e the density of the exhaust gas, g the gravitational acceleration, and D the inner diameter of the exhaust pipe. Assuming ideal gas, the density ratio is related to the temperature ratio as

$$\frac{\rho_a}{\rho_a - \rho_e} = \frac{T_e}{T_e - T_a}, \quad (2)$$

where T_a is the ambient temperature and T_e is the temperature of the exhaust gas.

The emission speed V of the exhaust gas is determined by matching the ratio of the inertia of the ambient flow to that of the exhaust gas

$$\frac{\rho_a U^2}{\rho_e V^2}. \quad (3)$$

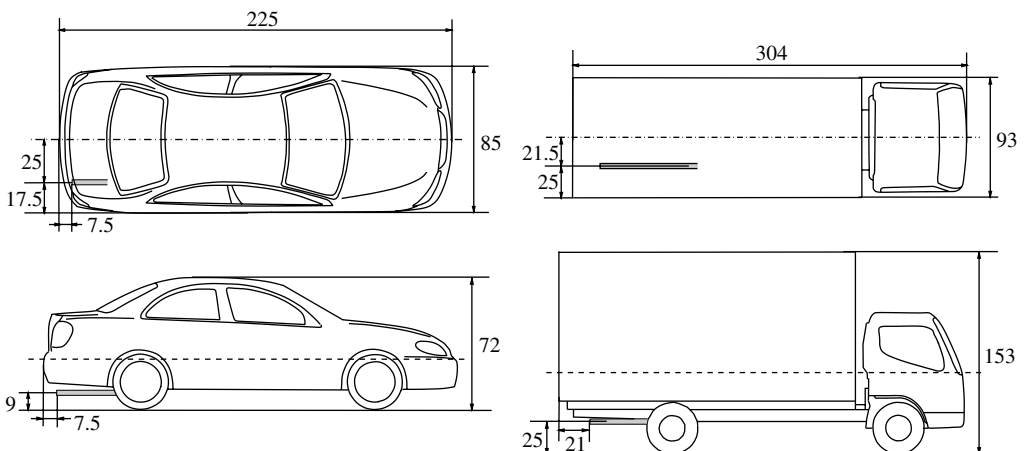


Fig. 2. Schematic drawings of the model vehicles. The unit of the length is mm. The shaded regions are the exhaust pipes. The dash-dot and the dashed lines indicate, respectively, the vertical and the horizontal sections for PIV measurement.

By matching this ratio, an alternative Froude number

$$Fr' = \sqrt{\frac{\rho_e V^2}{(\rho_a - \rho_e)gD}} \tag{4}$$

is also matched.

The above matching scheme is applied for $U \sim 1.5 \text{ m s}^{-1}$, a sufficiently large value for Reynolds number invariance of the velocity field (see Section 3), and the results are summarized in Table 1. The mixing ratio $\text{C}_2\text{H}_6:\text{He}:\text{N}_2$ is 60:40:0 for P and 5:50:45 for T. We note that the Reynolds number Re_D based on the pipe diameter is so small for P that the emitted exhaust plume might be laminar in the vicinity of the pipe exit.

The model vehicles are placed on a table (91 cm wide, 75 cm high and about 8 m long; Fig. 3) because, if placed on the wind-tunnel floor, the vehicles would be immersed in the

Table 1
Relevant parameters of the real and the model traffic conditions

	P (real)	P (model)	T (real)	T (model)
Length (m)	4.5	0.225	6.08	0.304
Width (m)	1.7	0.085	1.7	0.093
Height H (m)	1.44	0.072	3.0	0.153
U (m/s)	5.56	1.53	5.56	1.49
D (m)	0.043	0.0025	0.058	0.003
V (m/s)	1.85	0.55	17.55	5.27
Q_m (m^3/s)	–	1.62×10^{-6}	–	1.86×10^{-6}
T_e ($^\circ\text{C}$)	100		150	
T_a ($^\circ\text{C}$)	20		20	
$\text{C}_2\text{H}_6:\text{He}:\text{N}_2$		60:40:0		5:50:45
Re_H	5.2×10^5	7.1×10^3	1.1×10^6	1.4×10^4
Re_D	6.5×10^3	90	7.6×10^4	1020
Fr	17.14	17.14	13.07	13.07

The Reynolds numbers are defined by $Re_H = UH/\nu$ and $Re_D = UD/\nu$.

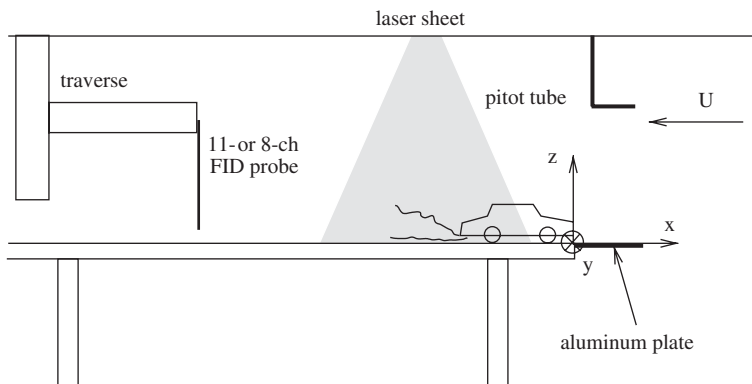


Fig. 3. A schematic view of the experimental configuration (not to scale).

turbulent boundary layer (about 20 cm thick around the measurement region) and the experiments would not represent vehicles moving into a quiescent ambient. To prevent abrupt growth of the boundary layer, a 1 mm-thick aluminum plate is attached at the upwind edge of the table top. Boundary layer, nonetheless, grows on the table top and reaches about 3 cm thick at about 1 m from the upwind edge of the table. When analyzing the experimental results, the effect of the boundary layer must be taken into account. Strictly speaking, the experimental configuration with the vehicles fixed on the table top does not represent the real traffic where vehicles move relative to the stationary road. In previous research targeted only at single vehicle properties [7,8,15], moving floor systems were used to create relative motion between the vehicles and the road. However, as will be described in our companion paper [13], our work is also intended for multi-vehicle queues which would require a considerably long and thus costly moving floor system. Our experimental scheme with no floor movement is a compromise adopted by some other authors [9,10]. We shall discuss the effect of floor movement later.

We adopt the Cartesian coordinate system shown in Fig. 3. The x direction is opposite to the mainstream, the y direction is in the spanwise (into the paper), and the z direction is perpendicular to the table surface. The origin is at the downwind edge ($x = 0$) of the aluminum plate, where the head of the vehicle is aligned, and at the centerline ($y = 0$) on the table top ($z = 0$). The velocity components in (x, y, z) directions are denoted by (u, v, w), respectively.

The velocity fields are measured by PIV (DANTEC Dynamics). A Nd-YAG laser sheet and glycerol mist are used for visualization. Both the vertical (xz -plane at $y = 0$) and horizontal (xy -plane at $z \sim 27.5$ mm for P and at $z \sim 62.5$ mm for T) sections are measured. The mean fluctuation fields are calculated from about 140 instantaneous velocity data sampled at 0.5 Hz. Due to the finite size of the calculation grid (10–17.5 mm in x and 5–9 mm in z), PIV underestimates the velocity fluctuations, 20–30% lower than the values measured by Laser Doppler Anemometry (LDA) at $\gtrsim 100$ Hz. For the vertical section at $y = 0$, we may assume $v = 0$ and define a streamfunction ψ satisfying $u = \partial\psi/\partial z$ and $w = -\partial\psi/\partial x$. Hence, the vertical section will be presented by contour maps of ψ .

The concentration fields of ethane are measured by FID (Kimoto Electric Co., Ltd.). The measurement probe consists of 11 (or 8) sampling pipes aligned in the y direction at 40 (or 20) mm intervals. The probe is mounted on a three-axis traverse. When the plume width is comparable to the spacing between the sampling pipes, the probe is shifted by half the spacing to obtain the values at intermediate points. The background concentration measured at a sufficiently upwind location is subtracted from the time-averaged data. The results are presented in ppm without normalization. If we assume that the concentration is proportional to Q/UL^2 where Q is the rate of emission and L is some length scale, the real-scale concentration can be recovered by

$$C_r = C_m \left(\frac{U_m}{U_r} \right) \left(\frac{L_m}{L_r} \right)^2 \left(\frac{Q_r}{Q_m} \right), \quad (5)$$

where the subscripts m and r denote ‘model’ and ‘real’ quantities, respectively. Since the length scale ratio $L_m/L_r = \frac{1}{20}$ is independent of the choice of the length L (vehicle height, pipe diameter, pipe height, etc.), the presentation in the raw value C_m is less confusing than a normalized presentation $C_m U_m L_m^2 / Q_m$ for which the choice of L_m may differ with experimental configurations. The emission rate Q_m of ethane is shown in Table 1.

3. Velocity fields

3.1. Critical Reynolds number

We first seek the critical Reynolds number beyond which the flow pattern remains similar. Although this paper deals with single-vehicle configurations only, our final objective is a queue of vehicles where the velocity defect and the turbulence due to the preceding vehicles affect the dispersion behavior. Since preceding vehicles reduce the speed of the oncoming flow, the critical Reynolds number (based on the mainstream speed U) determined with many preceding vehicles should be larger than that determined with less preceding vehicles. We assume that the turbulence generated by the preceding vehicles has minor effect on the mean flow pattern. This assumption will be justified later. As will be demonstrated in our companion paper [13], two preceding vehicles are sufficient to represent the effect of more preceding vehicles on diffusion behavior. Hence, the critical Reynolds number determined with more than two preceding vehicles is a *safe* overestimate.

Fig. 4 shows the streamfunction contours around a P behind a queue of nine P's at intervals (rear bumper to front bumper) of 50 cm for $U = 0.75, 1.5, 3.0 \text{ m s}^{-1}$. The intervals of the contours are proportional to U so that the difference in the flow patterns is discernible. We observe that the flow pattern changes considerably from $U = 0.75$ to 1.5 m s^{-1} ; the wake rolls up significantly for the former, but is suppressed vertically for

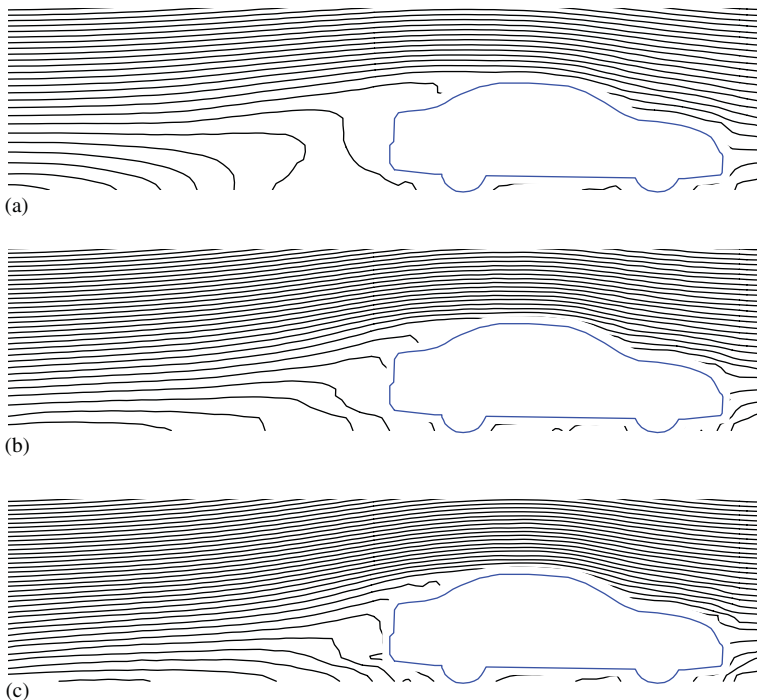


Fig. 4. Streamfunction contours at $y = 0$ around a passenger car (P) behind a queue of nine P's. The mainstream speed U (m s^{-1}) is (a) 0.75, (b) 1.5, (c) 3.0. The contour intervals are proportional to U .

$U \geq 1.5 \text{ m s}^{-1}$. The flow pattern for $U = 5.0 \text{ m s}^{-1}$ (not shown in the figure) is essentially the same as that for $U = 3.0 \text{ m s}^{-1}$. Hence, the critical Reynolds number lies between $0.75 \times H/\nu = 3.48 \times 10^3$ and $1.5 \times H/\nu = 6.97 \times 10^3$, where H is the vehicle height and $\nu = 1.55 \times 10^{-5} \text{ m}^2 \text{ s}^{-1}$ is the kinematic viscosity of air at 20°C . Note that the critical value falls in the range reported for surface mounted obstacles in turbulent boundary layers [16]. Because the streamlines for $U = 1.5 \text{ m s}^{-1}$ with nine preceding vehicles (Fig. 4b) are more elevated and sparse than those for the same U without preceding vehicles (see Fig. 5a), the critical Reynolds number is certainly a *safe* overestimate. Here, the above-mentioned assumption that the turbulence due to the preceding vehicles has minor effect on the wake is justified. If the turbulence were important, the boundary layer separation would be suppressed and the wake streamlines would be compressed toward the ground.

For T, we expect that the critical Reynolds number is surpassed for U well below 1.5 m s^{-1} because the length scale of T is larger than that of P. Indeed, the flow pattern around an isolated T is similar for $U = 0.75 \text{ m s}^{-1}$ (not shown) and for $U = 1.5 \text{ m s}^{-1}$ (see Fig. 6a). The roll-up flow behind T (Fig. 6a) is common to that observed by Lajos et al. [15] in a wind-tunnel study with a Reynolds number based on the vehicle width being up to 1.4×10^6 , close to the value of the real-scale truck.

In conclusion, the mainstream speed $U = 1.5 \text{ m s}^{-1}$ adopted in Table 1 for dynamical similarity of buoyancy and inertia is an appropriate choice for both P and T.

3.2. Mean and fluctuation velocity fields around isolated vehicles

We investigate the mean and fluctuation of the velocity fields behind isolated P and T. The fluctuation is represented by the standard deviation σ_u , σ_v , σ_w of the velocity components u , v , w , respectively. The fluctuation fields are shown by magnitude contours. For the mean velocity field, streamfunction contours (coincident with streamlines) are used for the xz plane whereas vector plots are used for the xy plane. The vehicles are placed on the table top, with the center of the front edge at $x = y = 0$.

Fig. 5 shows the vertical and horizontal sections of the mean and fluctuation fields behind P for $U = 1.5 \text{ m s}^{-1}$. For the mean field in the horizontal section (Fig. 5d), only vectors with magnitude smaller than 0.5 m s^{-1} are drawn since inclusion of the larger vectors would clutter the figure considerably. As already noted, the streamlines behind P are slightly lower and denser than those in the case with nine preceding P's (Fig. 4b).

In the vertical section of the fluctuation fields (Fig. 5b for σ_u , 5c for σ_w), large σ_u occurs above the rear window and below the rear bumper, and large σ_w above the trunk and behind the rear bumper. The large- σ_u regions correspond to the turbulence due to the large x direction shear, and the large- σ_w regions correspond to the vortices produced by the shear and spawned into the wake.

In the horizontal section (Fig. 5e for σ_u , 5f for σ_v), large- σ_u regions extend along the side of the vehicle body, and a large- σ_v region exists about one- to two-car-width behind P. The distribution of σ_u and σ_v represent the vertically suppressed but horizontally wide wake region. Along the path, the exhaust plume is first diffused in the vertical direction in the large- σ_w region (Fig. 5c), and then in the horizontal direction in the large- σ_v region (Fig. 5f). Since the wake region is relatively flat, the plume is expected to spread mainly in the horizontal.

Fig. 6 shows the vertical and horizontal sections of the mean and fluctuation fields behind T for $U = 1.5 \text{ m s}^{-1}$. A distinct feature is the roll-up flow in the near wake (Fig. 6a).

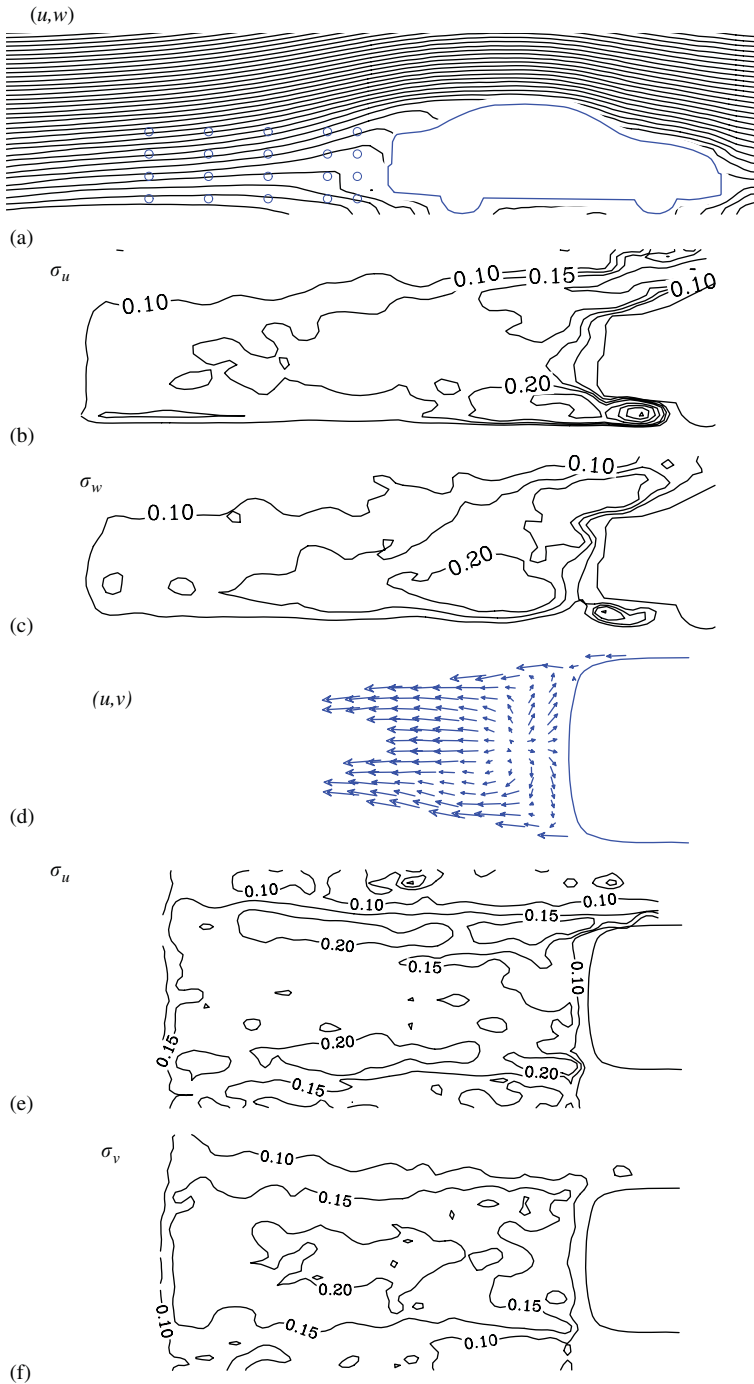


Fig. 5. The mean and the fluctuation fields of the flow behind a single P. (a) Streamfunction contours in the vertical section $y = 0$. The circles denote the measurement points by LDA. (b,c) Contour maps of the standard deviations σ_u and σ_w (m s^{-1}), respectively, at $y = 0$. (d) Mean velocity field in the horizontal section $z \sim 27.5$ mm. Only vectors with magnitude smaller than 0.5 m s^{-1} are drawn. (e,f) Contour maps of the standard deviations σ_u and σ_v (m s^{-1}), respectively, at $z \sim 27.5$ mm.

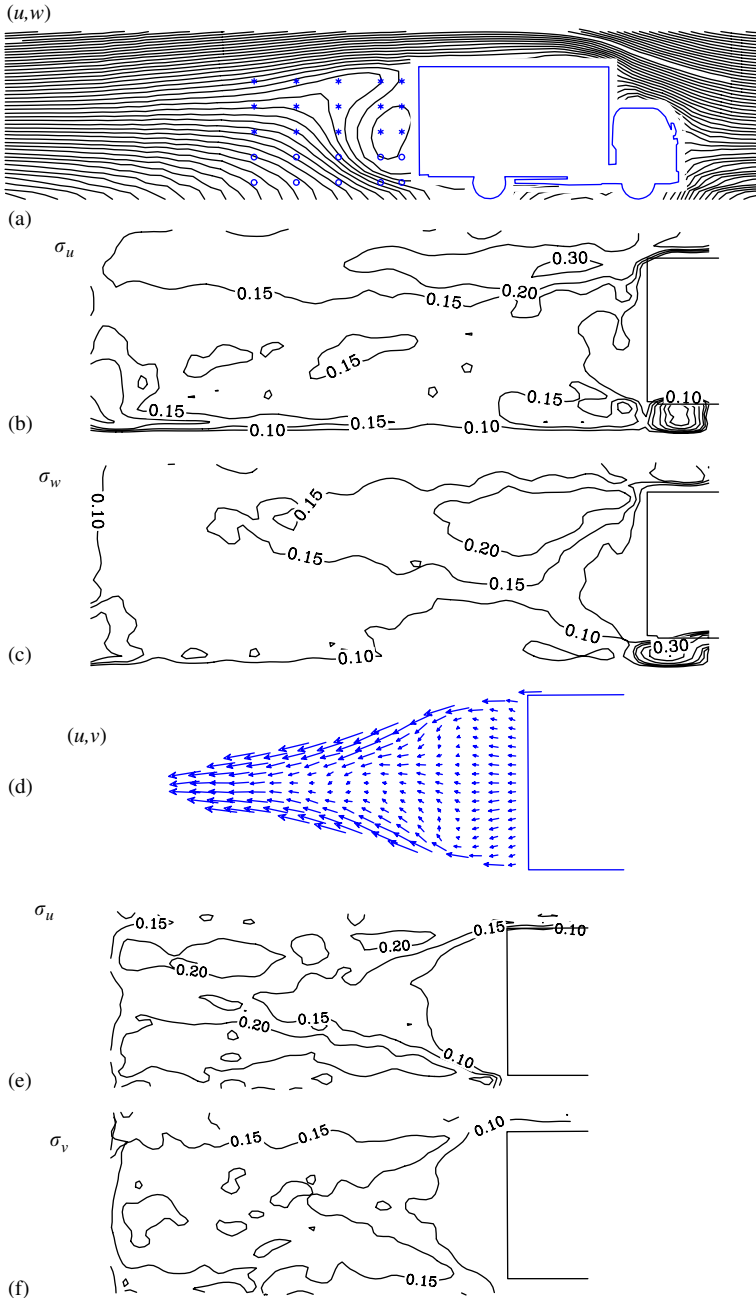


Fig. 6. The mean and the fluctuation fields of the flow behind a single T. (a) Streamfunction contours in the vertical section $y = 0$. The circles and asterisks denote the measurement points by LDA. (b,c) Contour maps of the standard deviations σ_u and σ_w (m s^{-1}), respectively, at $y = 0$. (d) Mean velocity field in the horizontal section $z \sim 62.5 \text{ mm}$. Only vectors with magnitude smaller than 0.4 m s^{-1} are drawn. (e,f) Contour maps of the standard deviations σ_u and σ_v (m s^{-1}), respectively, at $z \sim 62.5 \text{ mm}$.

For the mean field in the horizontal section (Fig. 6d), only vectors with magnitude smaller than 0.4 m s^{-1} are drawn. In contrast to the case with P, the wake behind T converges toward $y = 0$. Similar converging behavior was observed with P for $U = 0.75 \text{ m s}^{-1}$ (not shown) that exhibits roll-up streamlines (Fig. 4a) like T does (Fig. 6a).

In the vertical section of the fluctuation field (Fig. 6b for σ_u ; Fig. 6c for σ_w), the locations of large- σ_u regions are similar to those of P, i.e. behind the top of the freight space and below the rear bumper. As with P, a large- σ_w region exists below the upper large- σ_u region, but large σ_w is confined below the rear bumper. Hence, the exhaust plume is diffused vertically (probably horizontally as well) near the pipe exit, and is expanded vertically by the relatively calm roll-up flow (Fig. 6a). The upper part of the plume passes through the large- σ_v region about one- to two-car-width behind T (Fig. 6f), and also enter the large- σ_w region (Fig. 6c). Therefore, the plume would be spread significantly in the vertical.

Fig. 7 shows the vertical profiles of the streamwise velocity deficit at selected downwind distance x' from the rear end of the vehicles. We observe that the wake height is nearly constant and the deficit is non-zero near the floor unlike the real traffic in quiescent ambient. Although similarity theories are usually valid beyond $x'/H = O(10) \sim O(100)$ [17, p. 115], the magnitude of velocity deficit seems to vary as $(x'/H)^{-3/4}$, the prediction of the similarity theory by Eskridge and Hunt [18]. We remark that the theory of Eskridge and Hunt assumes no relative motion between the floor boundary and the mainstream, and the predicted velocity profile is distinctly different from our result.

At the points on $y = 0$ indicated in Figs. 5(a) and 6(a), the velocity was measured at sampling rate of about 100 Hz by LDA. The high sampling rate enables us to estimate the power spectra of the velocity fluctuation. Fig. 8 shows the representative power spectral density distribution for u . At the points denoted by circles (all the points behind P and the two bottom rows behind T), the spectra decay continuously with frequency (Fig. 8a), whereas at the points denoted by asterisks (the upper three rows behind T), there is a distinct peak at $f = 1.5 \text{ Hz}$ (Fig. 8b). This peak corresponds to the vortices shed behind the top of the freight space and generating the large- σ_w region (Fig. 6c). The Strouhal number fH/U is 0.15, smaller than 0.2 for obstacles in free stream.

4. Concentration fields behind single vehicles

We examine the concentration fields behind P or T for buoyant and neutral exhaust gas. The buoyant gas has the same constituent as shown in Table 1, and the neutral gas is made by replacing helium with nitrogen. In order to compare the widths of the exhaust plume, the Gaussian form (6) is fitted to the concentration distribution $C(y, z)$ in the yz plane at selected x positions. The Gaussian form is defined by

$$C(y, z) \sim \frac{Q_0}{2\pi U \sigma_y \sigma_z} \exp\left\{-\frac{(y - y_0)^2}{2\sigma_y^2}\right\} \left[\exp\left\{-\frac{(z - z_0)^2}{2\sigma_z^2}\right\} + \exp\left\{-\frac{(z + z_0)^2}{2\sigma_z^2}\right\} \right], \quad (6)$$

where the fitting parameters Q_0 , σ_y , σ_z , y_0 and z_0 are determined to minimize the rms difference of the both sides using the Nelder–Mead simplex method [19]. The plume width σ_y and σ_z generally increase with the downwind distance, and hence the concentration peak at the plume axis decreases with $|x|$. For both P and T, the lateral shift y_0 ranges in -24 to -29 mm , approximately the same as the tailpipe position (see Fig. 2). The parameter Q_0 corresponds to the emission rate Q_m . However, since the free-stream velocity U is used for

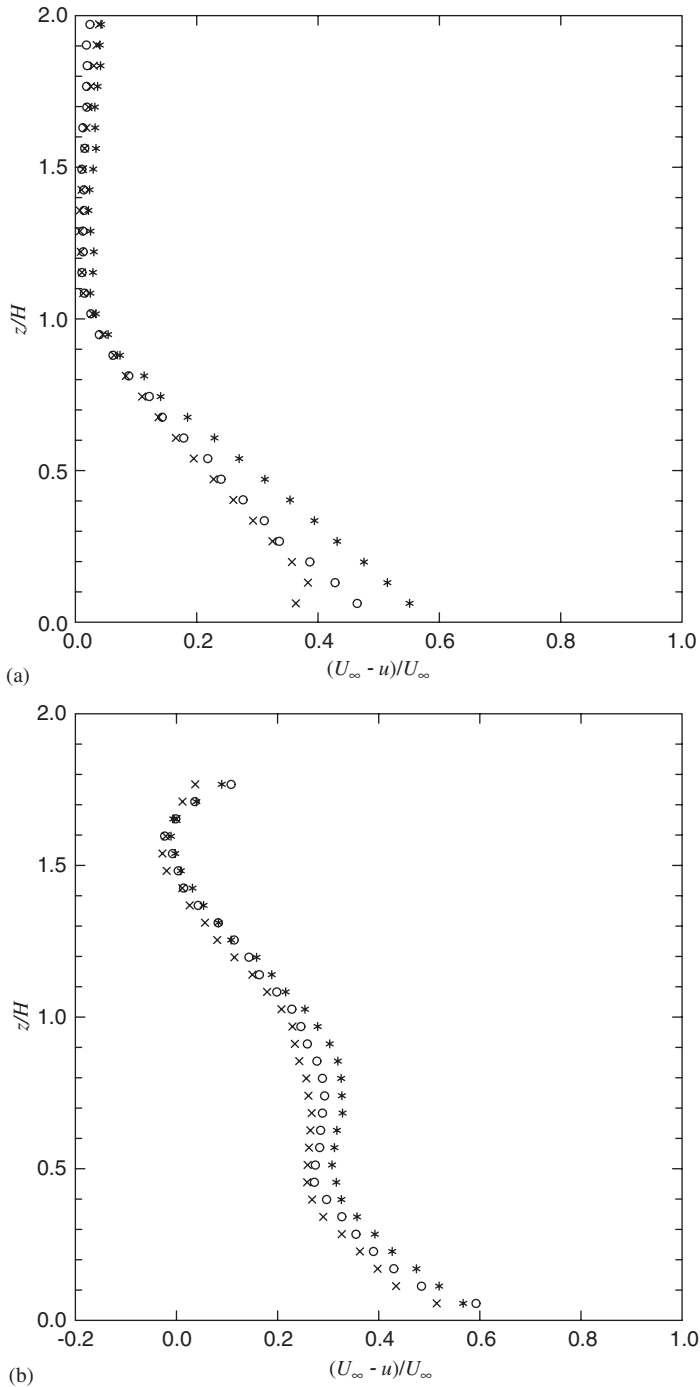


Fig. 7. Vertical profiles of velocity deficit for (a) P and (b) T. The normalized downwind distance x'/H from the rear end of the vehicles is (a) asterisk: 2.2, circle: 2.9, cross: 3.6; (b) asterisk: 3.7, circle: 4.4, cross: 5.1. U_∞ is the mainstream velocity.

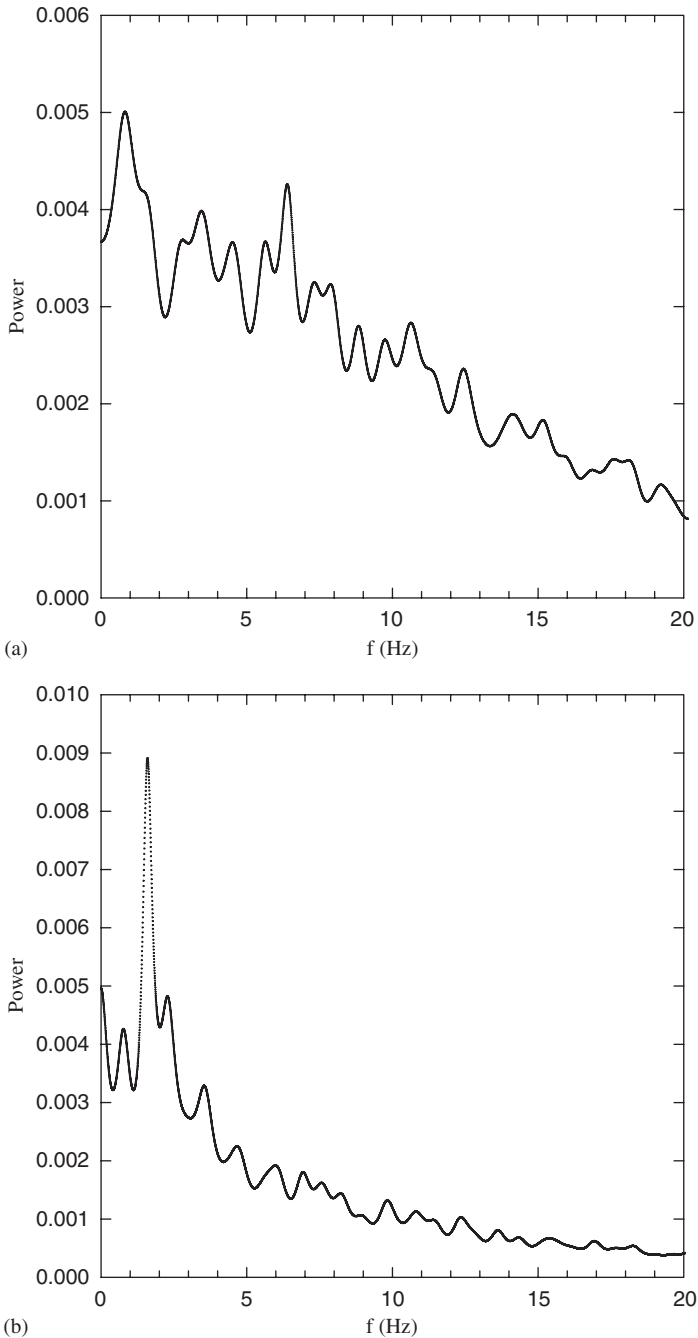


Fig. 8. Power spectral density distribution obtained from LDA data. The spectra are one-sided and are calculated by the maximum entropy method ($\text{lag} = \sqrt{\text{number-of-data}}$). (a) $(x, z) = (-265 \text{ mm}, 25 \text{ mm})$ (second row from the bottom, second column from the vehicle) behind P, (b) $(x, z) = (-404 \text{ mm}, 110 \text{ mm})$ (fourth row from the bottom, third column from the vehicle) behind T.

normalization instead of the reduced velocity in the wake, the obtained values of Q_0 is about 60–100% larger than Q_m (cf. Table 1). Hence, the individual values of Q_0 and U do not have much physical significance. Alternatively, the combination $Q_0/2\pi U$ may be viewed as a mere scaling factor.

Fig. 9 shows the concentration contours in yz sections for P with the buoyant gas. The dashed contours are the optimal fit of the Gaussian distribution. Note that the contour interval is 25 ppm for (a,b) and 50 ppm for (c). Near the vehicle (Fig. 9c, $x = -525$ mm), we observe that the concentration peak is close to the pipe position ($y = -25$ mm) at lower z but shifts toward the center ($y = 0$) at higher z . This distribution can be explained as

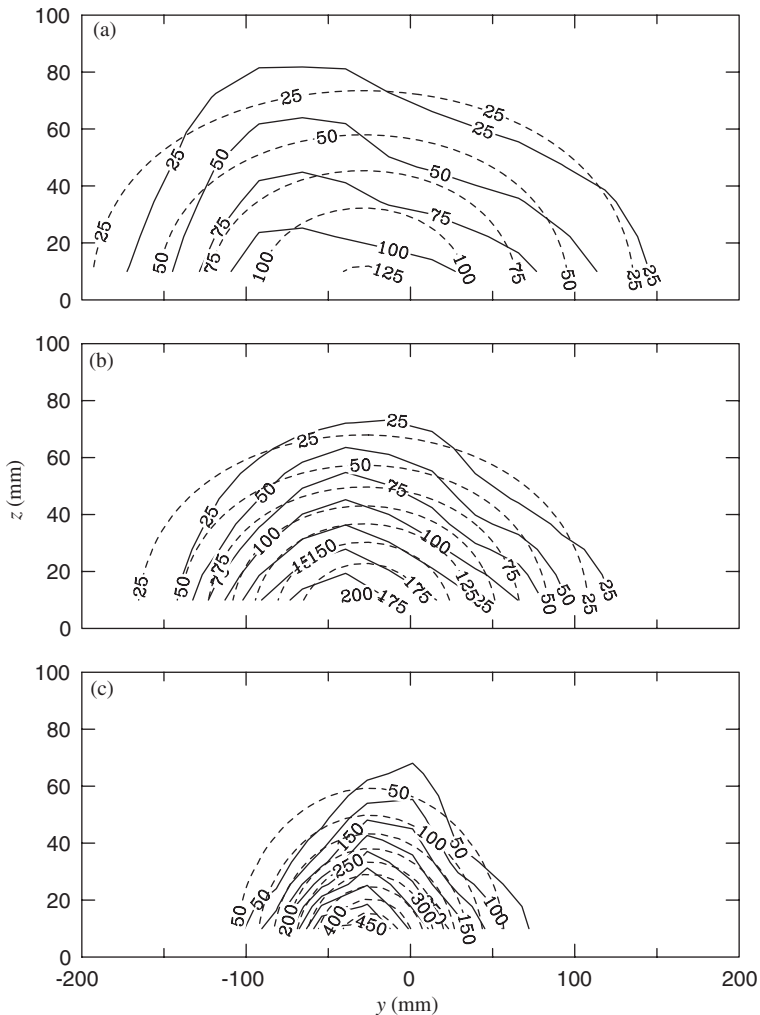


Fig. 9. The concentration contours in the yz section behind a single P with the buoyant exhaust gas. The x (mm) coordinate (origin at the vehicle head) is (a) -1775 , (b) -1050 , (c) -525 . The solid lines are the measured data and the dashed lines are the optimal fit to the Gaussian form (6). Note that the contour interval is 25 ppm for (a,b) and 50 ppm for (c).

follows. Near the pipe exit, the exhaust plume is raised slightly by the mean flow (Fig. 5a) but is soon mixed (probably mostly vertically) in the wake turbulence (Fig. 5c); together with reflection at $z = 0$, the concentration peak appears at the pipe y position near the table top; the upper part of the plume is brought toward the center ($y = 0$) by the horizontally converging mean flow (Fig. 5d at $z \sim 27.5$ mm) and is also mixed horizontally (Fig. 5f), and hence tends to symmetric about $y = 0$. We emphasize that this retrospective explanation is subject to the relative importance of the contributing factors (plume raising, mixing, convergence, etc.), and cannot be extended to predict the concentration field merely from the velocity field. In the far wake (Fig. 9b at $x = -1050$ mm, 9c at $x = -1775$ mm), the peak concentration at lower z diffuses, and the bias toward negative y prevails through the plume height.

With the neutral gas, the concentration contours are found almost identical to those with the buoyant gas. In an experiment where the exhaust gas was emitted from a bare pipe without the vehicle body, we found that the difference in the concentration fields between the buoyant and the neutral gas is also within experimental errors. Hence, the cause of the identity is solely attributable to the relatively small buoyancy flux of the P-type exhaust gas.

Fig. 10 shows the concentration contours in yz sections for T with the buoyant (Fig. 10i) and the neutral gas (Fig. 10ii). As with P, the concentration peak is close to the pipe y position at lower z but shifts toward the center ($y = 0$) at higher z . This contour shape can be explained qualitatively by a scenario similar to that for P, but the roll-up flow behind T raises the plume considerably higher than for P, and hence the concentration contour has a conspicuous bulge around $y = 0$.

In contrast to P, the concentration contours for the buoyant gas is more vertically stretched than those for the neutral gas. We note, however, that the plume axis lies on the table top ($z_0 \sim 0$) for both the buoyant and the neutral cases. As shown in Fig. 11(ii-c, dashed lines), the buoyant plume rises significantly higher than the neutral plume when the exhaust gas is emitted from a bare pipe without the vehicle body. We speculate that the vigorous mixing near the pipe exit (Fig. 6c) brings the plume axis down to the table top irrespective of the buoyancy of the gas. That the pipe exit is more receded for T than for P (see Fig. 2) also enhances this effect. The buoyancy, however, affects the subsequent path of the upper part of the plume: a small height difference near the pipe exit results in significant difference in the path along the roll-up streamlines (see Fig. 6a). Hence, larger portion of the buoyant plume than of the neutral plume enters the region of large σ_u and σ_w (Fig. 6b,c), and the turbulent mixing results in the taller concentration contours in the yz plane.

Fig. 11 summarizes the x -dependence of σ_y , σ_z and z_0 in Eq. (6). For comparison, results of emission from bare pipes without the vehicle bodies are shown by dashed lines. By comparing with the bare pipe cases, the effect of the boundary layer on the table top can be canceled. Features including already mentioned ones are listed below.

- (1) The horizontal width (σ_y) is comparable for P (Fig. 11i-a) and T (Fig. 11ii-a), while the vertical width (σ_z) for T (Fig. 11ii-b) is significantly larger than that for P (Fig. 11i-b).
- (2) For both P and T, the horizontal width (σ_y) grows faster than in the bare-pipe cases, while the vertical width (σ_z) maintains the difference from the bare-pipe case in the near wake ($x = -525$ mm for P, $x = -604$ mm for T). This behavior reflects the characteristics of the fluctuation field that large- σ_w regions are confined near the rear

side of the vehicles (see Fig. 5c and 6c), while large- σ_v regions extends far and wide (see Fig. 5f and 6f).

- (3) For P, the plume axis (z_0) rises to a height comparable to that in the bare-pipe case (Fig. 11i-c), while the plume axis for T is on the table top, much lower than in the bare-pipe case (Fig. 11ii-c). We suppose that the landing of the plume for T is caused by the vigorous vertical mixing near the pipe exit.
- (4) The effect of buoyancy appears in σ_z for T in the near wake ($x \lesssim 604$ in Fig. 11ii-b). As mentioned above, this is due to the shape of the roll-up streamlines and vigorous vertical mixing in the upper part of the wake.

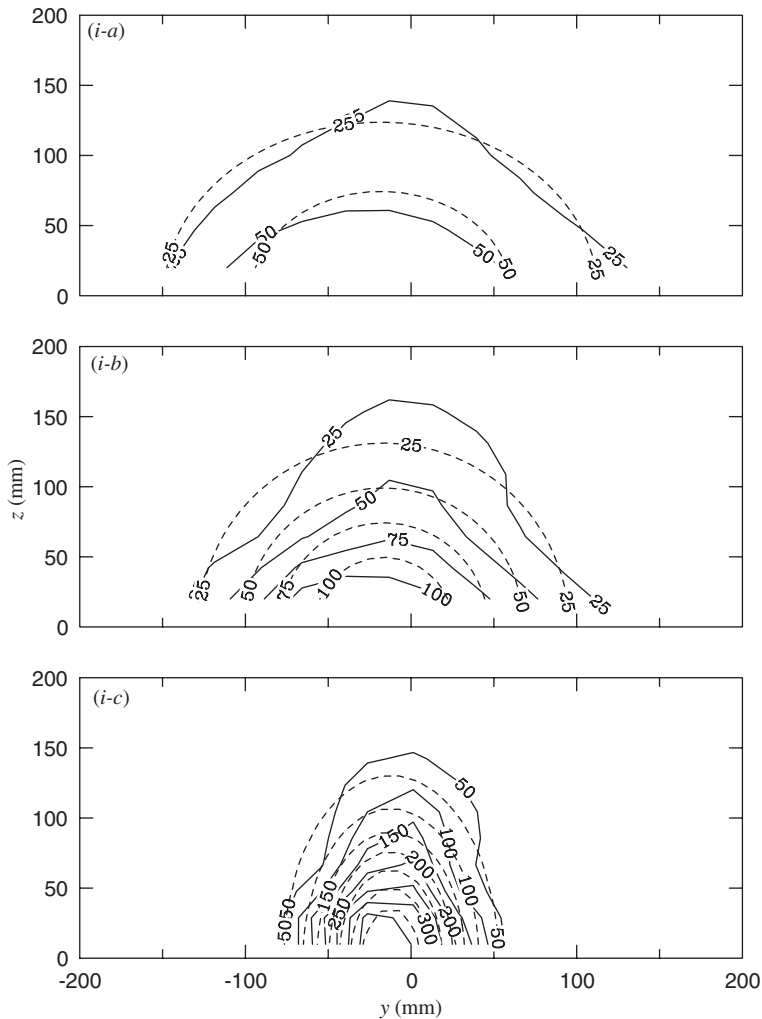


Fig. 10. The concentration contours in the yz section behind a single T with (i) the buoyant and (ii) the neutral exhaust gas. The x (mm) coordinate (origin at the vehicle head) is (a) -1829 , (b) -1124 , (c) -604 . The solid lines are the measured data and the dashed lines are the optimal fit to the Gaussian form (6). Note that the contour interval is 25 ppm for (a,b) and 50 ppm for (c).

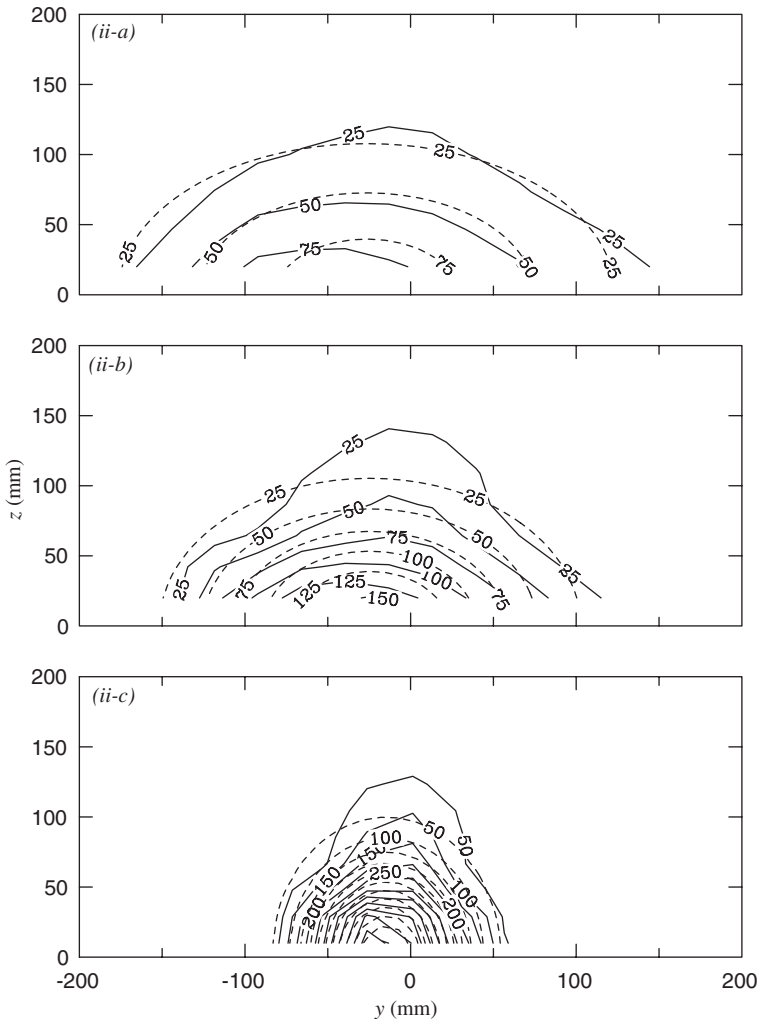


Fig. 10. (Continued)

5. Discussion

As a first step toward understanding the effect of moving traffic on exhaust gas dispersion, we investigated the velocity field around typical vehicles and the concentration field of exhaust gas behind isolated vehicles. We found that the presence of the vehicle body enhances dispersion considerably and that the concentration field reflects the characteristics of the mean and fluctuation fields of the flow around the vehicles. The buoyancy of the exhaust gas is found to have minor effect on the dispersion behavior except where the velocity field amplifies the vertical displacement as for T.

Our results are directly relevant to sparsely distributed vehicles in calm ambient. The degree of diffusion in the near-wake region where similarity theories do not work can be

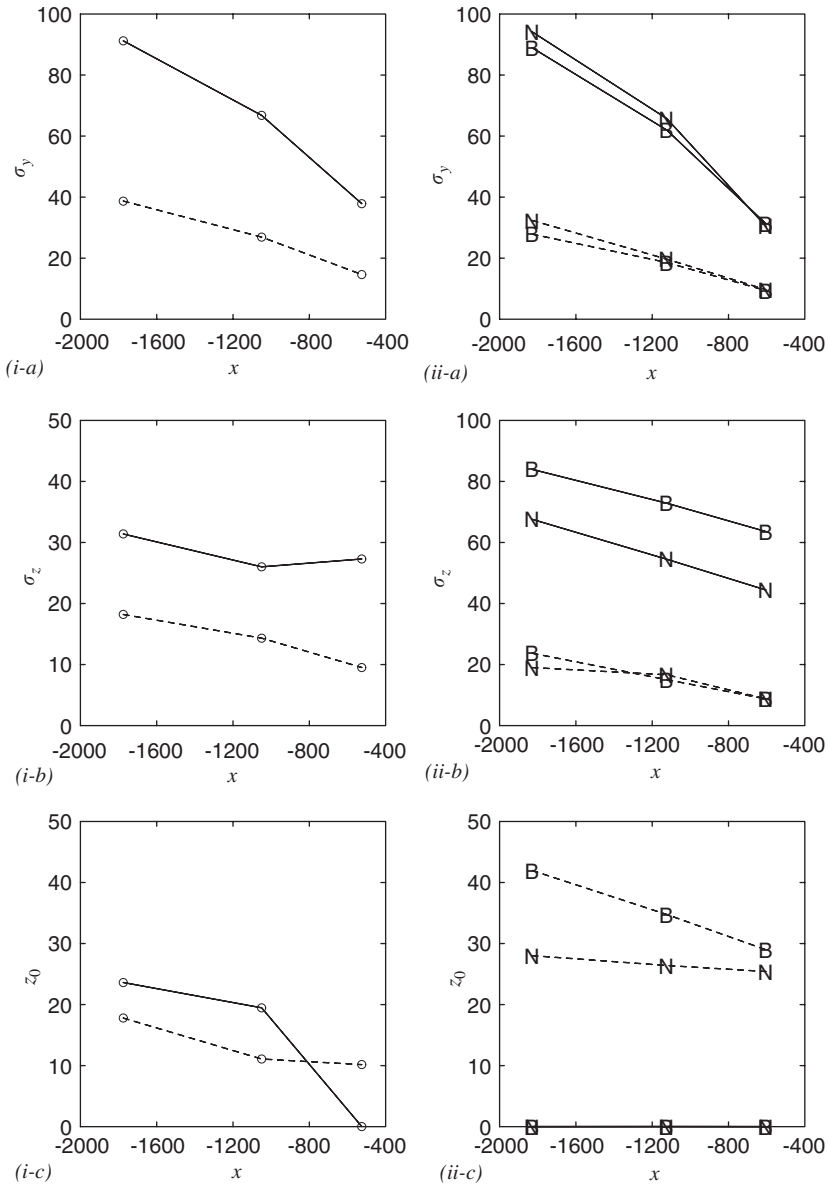


Fig. 11. The Gaussian fitting parameters σ_y , σ_z and z_0 for (i) the passenger car (P) and (ii) the truck (T). The units are all in mm. The dotted lines denote the results for the bare pipe experiments without the vehicle bodies. In (ii), the marks ‘B’ and ‘N’ represent ‘buoyant’ and ‘neutral’ gas, respectively.

incorporated in pollution models. Also, the results provide useful information for vehicle designers. For example, the velocity and fluctuation field around the vehicles suggest that the exhaust gas diffusion would be suppressed when the exhaust pipe is installed on the top of T (though not presented here, we did confirm this behavior experimentally). Another

use of our results is as the basis for the study of multi-vehicle queues treated in our companion paper [13].

Although dynamical similarity has been carefully enforced in our experiments, some cautionary remarks must be made. First, the table top in our experiments is stationary although the ground must move at the same speed as the mainstream wind for a correct simulation of the real traffic in a quiescent ambient. The stationary boundary has two effects: modification of the wake flow and mixing in the boundary layer.

As for the former effect, Lajos et al. [15] in an experiment with a moving floor found that the stagnation point of the roll-up flow behind a model bus is lower when the road is moving at the same speed as the mainstream than when the road is stationary. Hence, on the real road, the vertical width σ_z of the exhaust plume for T would be smaller than in our experiments. However, for a relatively low-profile vehicles like P, Hackett et al. [8] showed that the movement of the road has insignificant effect on the wake flow. Hence, the effect on the dispersion behavior in the near wake of P is likely to be small.

Besides the mean wake field, the fluctuation field may be altered by the boundary condition on $z = 0$. Although no data are available for comparison, we expect that the most-affected region is near the rear bumper where the exhaust plume is mixed upon emission. Since initial mixing is important in determining the subsequent evolution of the exhaust plume, the fluctuation in the moving boundary experiments should be measured and compared with our results.

The other consequence of the stationary boundary is the turbulent boundary layer (thickness ~ 30 mm at $x \sim -1$ m) that promotes mixing near the table top, expanding especially the horizontal width σ_y of the plume. This effect is observed in Fig. 11 where $\sigma_y > \sigma_z$ for the bare P-type exhaust pipe (Fig. 11i-a,i-b; dashed lines) and $\sigma_y \sim \sigma_z$ for the bare T-type exhaust pipe (Fig. 11ii-a,ii-b; dashed lines). For the former, the plume remains inside the boundary layer ($z_0 \lesssim 20$ mm, Fig. 11i-c) due to the low pipe height ($z = 9$ mm) and the small buoyancy; for the latter, the plume rises above the boundary layer ($z_0 \gtrsim 30$ mm, Fig. 11ii-c) due to the high pipe height ($z = 25$ mm) and the large buoyancy. However, since the vertical width σ_z of the exhaust plume behind vehicles is larger than the boundary layer thickness (Fig. 11i-b,ii-b), the effect of the boundary layer is limited to the lower part of the plume. The values of σ_y obtained in our experiments, nonetheless, should be viewed as overestimate.

Another remark is about the heat from vehicle engines. In urban traffic, the heat flux is estimated to be $O(10)$ kJ s⁻¹, which might generate sufficiently strong natural convection that may increase σ_z and z_0 , especially when the ambient wind is weak. In order to include this effect, an operational model CALINE4 [2] modifies the local atmospheric stability class, and another model CPBM [20] assumes that the vehicle heat contributes linearly to the velocity fluctuation. Proper experiments are desired to validate such empirical procedures.

Acknowledgments

This research was conducted as a project of Petroleum Energy Center with a financial support by Japanese Ministry of Economy, Trade and Industry. We appreciate the technical assistance of Mr. T. Kawata at Forum Engineering Inc.

References

- [1] S. Vardoulakis, B.E.A. Fisher, K. Pericleous, N. Gonzalez-Flesca, Modelling air quality in street canyons: a review, *Atmos. Environ.* 37 (2003) 155–182.
- [2] P.E. Benson, A review of the development and application of the caline3 and 4 models, *Atmos. Environ.* 26B (1992) 379–390.
- [3] H. Kono, S. Ito, A micro-scale dispersion model for motor vehicle exhaust gas in urban areas—OMG VOLUME-SOURCE model, *Atmos. Environ.* 24B (1990) 243–251.
- [4] R. Berkowicz, OSPM—a parametrised street pollution model, *Environ. Monit. Assessment* 65 (2000) 323–331.
- [5] Y. Yoshikawa, H. Kunimi, Numerical simulation model for predicting air quality along urban main roads: first report, development of atmospheric diffusion model, *Heat Transfer-Jpn. Res.* 27 (1998) 483–496.
- [6] A.G. Venetsanos, J.G. Bartzis, S. Andronopoulos, D. Vlachogiannis, Vehicle effects on street canyon air pollution pattern, in: *Ninth International Conference on Modeling, Monitoring and Management of Air Pollution*, WIT Press, 2001, pp. 193–202.
- [7] R.E. Eskridge, R.S. Thompson, Experimental and theoretical study of the wake of a block-shaped vehicle in a shear-free boundary flow, *Atmos. Environ.* 16 (1982) 2821–2836.
- [8] J.E. Hackett, J.E. Williams, J.B. Baker, S.B. Wallis, On the influence of ground movement and wheel rotation in tests on modern car shapes, Technical Report 870245, SAE Technical Paper Series, 1987.
- [9] R.E. Eskridge, S.T. Rao, Turbulent diffusion behind vehicles: experimentally determined turbulence mixing parameters, *Atmos. Environ.* 20 (1986) 851–860.
- [10] M.J. Clifford, R. Clarke, S.B. Riffat, Local aspects of vehicular pollution, *Atmos. Environ.* 31 (1997) 271–276.
- [11] M. Khare, K.K. Chaudhry, R.M.M. Gowda, K. Ahmad, Heterogeneous traffic induced effects on vertical dispersion parameter in the near field of roadways—a wind tunnel study, *Environ. Modeling Assessment* 7 (2002) 9–15.
- [12] K. Ahmad, M. Khare, K.K. Chaudhry, Model vehicle movement system in wind tunnels for exhaust dispersion studies under various urban street configurations, *J. Wind Eng. Ind. Aerodyn.* 90 (2002) 1051–1064.
- [13] I. Kanda, K. Uehara, Y. Yamao, Y. Yoshikawa, T. Morikawa, A wind-tunnel study on exhaust-gas dispersion from road vehicles—Part II: effect of vehicle queues, *J. Wind Eng. Ind. Aerodyn.*, submitted for publication.
- [14] Y. Ogawa, P.G. Diosey, K. Uehara, H. Ueda, A wind tunnel for studying the effects of thermal stratification in the atmosphere, *Atmos. Environ.* 15 (1981) 807–821.
- [15] T. Lajos, L. Preszler, L. Finta, Effect of moving ground simulation on the flow past bus models, *J. Wind Eng. Ind. Aerodyn.* 22 (1986) 271–277.
- [16] K. Uehara, S. Wakamatsu, R. Ooka, Studies on critical Reynolds number indices for wind-tunnel experiments on flow within urban areas, *Boundary-Layer Meteorol.* 107 (2003) 353–370.
- [17] H. Tennekes, J.L. Lumley, *A First Course in Turbulence*, MIT Press, Cambridge, MA, 1972.
- [18] R.E. Eskridge, J.C.R. Hunt, Highway modeling. Part I: prediction of velocity and turbulence fields in the wake of vehicles, *J. Appl. Meteorol.* 18 (1979) 387–400.
- [19] M. Galassi, J. Davies, J. Theiler, B. Gough, G. Jungman, M. Booth, F. Rossi, *GNU Scientific Library: Reference Manual*, second ed., Network Theory Ltd., 2003.
- [20] R.J. Yamartino, G. Wiegand, Development and evaluation of simple models for the flow, turbulence and pollutant concentration fields within an urban street canyon, *Atmos. Environ.* 20 (1986) 2137–2156.